Section 1:
Physics and Detector Performance Metrics

GlueX-doc-999-v2

GlueX/Hall D Conceptual Design Report

1 Physics and Detector Performance Metrics

We start this report on GlueX detector by discussing the physics goals of the GlueX project – mapping the spectrum of gluonic excitations starting with exotic hybrid mesons. We show that the search for exotic mesons depends critically on detecting and measuring the four-momenta of charged particles and photons resulting from the decays of photoproduced mesons. As will be discussed in this report, the majority of the final states that will be studied in GlueX involve a combination of both charged particles and photons. As such, in discussing the performance of the detector, it makes little sense to try and separate these issues.

This report includes information on the electromagnetic calorimetry needed to detect and measure those photons, the tracking chambers that are used to reconstruct the charged particles in GlueX . In addition, a time-of-flight wall is used in conjunction with measurements for other detectors to carry out some particle identification in GlueX. It is the physics goals that determine the performance metrics of the detectors. This includes the granularity, energy, position and timing resolution, and energy thresholds of the calorimeter. It also includes the position resolution of the drift chambers in conjunction with the charged particle tracking which is used to take advantage of timing measurements in both the barrel calorimeter and the time-of-flight wall. Information from the calorimetry will also be used for separating protons from pions and also to provide some information on recoil neutrons. In the central region of the detector, dE/dx measurements in central drift chamber (CDC) will be used to identify π, K and p for low momentum (under $450\,MeV/c$) which are likely to only be seen in the tracking chambers.

The GlueX detector consists of a cylindrical drift chamber (CDC) in the upstream half of a $\sim 4\,m$ long, $2.25\,T$ solenoidal magnet followed by four packages of planar drift chambers (FDC) in the down-stream half of the magnet. A barrel calorimeter (BCAL) surrounds the target and tracking chambers inside the magnet and a down-stream planar calorimeter (FCAL) provides coverage for photons exiting the down-stream hole of the magnet. A time-of-flight wall sits directly in front of the FCAL and space has been left between the end of the magnet and the time-of-flight to accommodate a future particle identification system (probably a ring imaging Chernkov counter).

The requirements on acceptance and on energy, position and timing resolution are driven by the need to identify exclusive reactions in order to perform the amplitude analyses that will extract meson J^{PC} quantum numbers and on the need to be sensitive to a variety of meson decay modes. Generally speaking, good amplitude analysis needs a large and uniform acceptance detector with good resolution for cleanly separating final state, which reduces background leakage into the reactions of interest.

The GlueX does have nearly 4π acceptance for both charged particles and photons. However, that acceptance is not completely uniform in all variables. As with any amplitude analysis, this means that the detector simulation package will need to be able to accurately reproduce the overall detector acceptance. Areas of reduced acceptance include very low momentum charged particles (protons under $300\,MeV/c$ and πs under $150\,MeV/c$, low energy photons, and photons going into the overlap region of the two calorimeters. Substantial work has gone into identifying these problematic regions and minimizing them by design optimization in the detector.

1.1 Physics motivation: the search for exotic mesons

1.1.1 QCD and light meson spectroscopy

The observation, nearly four decades ago, that mesons are grouped in nonets, each characterized by unique values of J^{PC} – spin (J), parity (P) and charge conjugation (C) quantum numbers – led to the development of the quark model. Within this picture, mesons are bound states of a quark (q) and antiquark ($\bar{q}$). The three light-quark flavors (*up*, *down* and *strange*) suffice to explain the spectroscopy of most – but not all – of the lighter-mass mesons (below 3 GeV/c^2) that do not explicitly carry heavy flavors (charm or beauty). Early observations yielded only those J^{PC} quantum numbers consistent with a fermion-antifermion bound state. The J^{PC} quantum numbers of a $q\bar{q}$ system with total quark spin, $\vec{S}$, and relative angular momentum, $\vec{L}$, are determined as follows: $\vec{J} = \vec{L} + \vec{S}$, $P = (-1)^{L+1}$ and $C = (-1)^{L+S}$. Thus J^{PC} quantum numbers such as 0^{--}, 0^{+-}, 1^{-+} and 2^{+-} are not allowed and are called *exotic* in this context.

Our understanding of how quarks form mesons has evolved within quantum chromodynamics (QCD) and we now expect a richer spectrum of mesons that takes into account not only the quark degrees of freedom but also the gluonic degrees of freedom. Gluonic mesons with no quarks (*glueballs*) are expected. These are bound states of pure glue and since the quantum numbers of low-lying glueballs (below 4 GeV/c^2) are not exotic, they should manifest themselves as extraneous states that cannot be accommodated within $q\bar{q}$ nonets. But their unambiguous identification is complicated by the fact that they can mix with $q\bar{q}$. Excitations of the gluonic field binding the quarks can also give rise to so-called *hybrid* mesons that can be viewed as bound states of a quark, antiquark and valence gluon ($q\bar{q}g$). An alternative picture of hybrid mesons, one supported by lattice QCD [9], is one in which a gluonic flux tube forms between the quark and antiquark and the excitations of this flux tube lead to so-called *hybrid* mesons. Actually the idea of flux tubes, or strings connecting the quarks, originated in the early 1970's [10] to explain the observed linear dependence of the mass-squared of hadrons on spin (Regge trajectories). Conventional $q\bar{q}$ mesons arise when the flux tube is in its ground state. Hybrid mesons arise when the flux tube is excited and some hybrid mesons can have a unique signature, exotic J^{PC}, and the spectroscopy of these exotic hybrid mesons is simplified because they do not mix with conventional $q\bar{q}$ states.

The level splitting between the ground state flux tube and the first excited transverse modes is π/r, where r is the separation between the quarks, so the hybrid spectrum should lie about 1 GeV/c^2 above the ground state spectrum. While the flux-tube model [11] has all hybrid nonets degenerate in mass, from lattice gauge calculations [12], one expects the lightest $J^{PC} = 1^{-+}$ exotic hybrid to have a mass of about 1.9 GeV/c^2. In this discussion the motion of the quarks was ignored, but we know from general principles [11] that an approximation that ignores the impact of the flux tube excitation and quark motion on each other seems to work quite well. It should be noted, also, the in the large-N_c limit of QCD, exotic hybrids are expected to have narrow widths, comparable to $q\bar{q}$ states [13].

In the coming years there will be significant computational resources dedicated to understanding non-perturbative QCD including confinement using lattice techniques. The prediction of the hybrid spectrum, including decays, will be a key part of this program but experimental data will be needed to verify these calculations. The spectroscopy of exotic mesons provides a clean and attractive starting point for the study of gluonic excitations.

The GlueX experiment is designed to collect high quality and high statistics data on the photoproduction of light mesons. As part of the program of identifying exotic hybrid mesons, these data will also be used to understand the conventional meson spectrum including the poorly understood excited vector mesons.

1.1.2 Using linearly polarized photons

There are tantalizing suggestions, mainly from experiments using beams of π mesons, that exotic hybrid mesons exist. The evidence is by no means clear cut, owing in part, to the apparently small production rates for these states in the decay channels examined. It is safe to conclude that the extensive data collected to date with π probes have not uncovered the hybrid meson spectrum. (A recent paper by E. Klempt and A. Zaitsev gives an encyclopedic and critical overview of the current experimental situation with regard to searches for glueballs, hybrids and multiquark mesons[14].) Models, like the flux-tube model, however, indicate the photon is a probe that should be particularly effective in producing exotic hybrids, but data on photoproduction of light mesons are sparse indeed.

The first excited transverse modes of the flux tube are degenerate and correspond to clockwise or counterclockwise rotations of the flux tube about the axis joining the quark and antiquark fixed in space with $J = 1$ [11]. Linear combinations of these two modes are eigenstates of parity and lead to $J^{PC} = 1^{+-}$ and $J^{PC} = 1^{-+}$ for the excited flux tube. When these quantum numbers are combined with those of the $q\bar{q}$ with $\vec{L} = 0$ and $\vec{S} = 1$ (quark spins aligned) three of the six possible J^{PC} have exotic combinations: 0^{+-}, 1^{-+} and 2^{+-}. A photon probe is a virtual $q\bar{q}$ with quark spins aligned. In contrast when the $q\bar{q}$ have $\vec{L} = 0$ and $\vec{S} = 0$ (spins anti-aligned), the resulting quantum numbers of the hybrid meson are not exotic. Pion probes are $q\bar{q}$ with quark spins anti-aligned. If we view one outcome of the scattering process as exciting the flux tube binding the quarks in the probe, the suppression of exotic hybrids in π-induced reactions is not surprising – a spin flip of one of the quarks is required followed by the excitation of the flux tube. In contrast the spins

of the virtual quarks in the photon probe are properly aligned to lead to exotic hybrids. Phenomenological studies quantitatively support this picture predicting that the photoproduction cross-sections for exotic mesons are comparable to those for conventional mesons [15].

Determining the quantum numbers of mesons produced in the GlueX experiment will require an amplitude analysis based on measuring the energy and momentum of their decay products. Linear polarization of the incident photon is required for a precision amplitude analysis to identify exotic quantum numbers, to understand details of the production mechanism of exotic and conventional mesons and to remove backgrounds due to conventional processes. Linear polarization will be achieved using the coherent bremsstrahlung technique.

For the GlueX solenoid-based detector system, given the required mass reach required for mapping the spectrum of exotic hybrid mesons, a photon energy of ≈ 9 GeV is ideal. To achieve the requisite degree of linear polarization for 9 GeV photons using coherent bremsstrahlung requires a minimum electron energy of 12 GeV.

1.1.3 Expected decay modes of exotic hybrid mesons

Table 1.1 lists predicted J^{PC} exotic mesons and their decay modes. According to the flux tube model and verified by lattice QCD [16], the preferred decay modes for exotic hybrids are into $(q\bar{q})_P + (q\bar{q})_S$ mesons such as $b_1 + \pi$ or $f_1 + \pi$. Table 1.2 lists candidate exotic $J^{PC} = 1^{-+}$ state for which evidence has been claimed. The purported exotic states include decay modes into $b_1\pi$ or $f_1\pi$ as well as decay modes into $\eta\pi$ and $\eta'\pi$. The dominant branching fractions for meson states listed among the decay products are summarized in Table 1.3. Clearly, exotic meson spectroscopy requires the ability to detect and measure charged particles as well as π^0 and η mesons.

Some of the preferred or observed exotic hybrid decay modes listed in Tables 1.1 and 1.2 do not necessarily involve π^0 mesons, *e.g.* the $\rho\pi$ or $a_2\pi$ modes – these can have final states that only involve $\pi^\pm$ such as $(\rho\pi)^+ \to \pi^+\pi^+\pi^-$. But if a state decays into such an all charged π system, having the isospin partners available, such as $(\rho\pi)^+ \to \pi^+\pi^0\pi^0$ provides important isospin consistency checks of the amplitude analysis and understanding of the detector acceptance.

Exotic Meson	J^{PC}	I	G	Possible Modes
b_0	0^{+-}	1	+	
h_0	0^{+-}	0	−	$b_1\pi$
π_1	1^{-+}	1	−	$\rho\pi$, $b_1\pi$
η_1	1^{-+}	0	+	$a_2\pi$
b_2	2^{+-}	1	+	$a_2\pi$
h_2	2^{+-}	0	−	$\rho\pi$, $b_1\pi$

Table 1.1: Predicted J^{PC} exotic hybrid mesons and their expected decay modes. See Table 1.3 for decay modes of the b_1 and a_2 mesons.

Exotic Meson Candidate	Decay Mode
$\pi_1(1400)$	$\pi^-\eta$
	$\pi^0\eta$
$\pi_1(1600)$	$\rho^0\pi^-$
	$\eta'\pi^-$
$\pi_1(1600/2000)$	$b_1\pi$
	$f_1\pi$

Table 1.2: Reported $J^{PC} = 1^{-+}$ exotic hybrid mesons and their decay modes. See Table 1.3 for decay modes of the η', b_1 and f_1 mesons. Source: 2006 Review of Particle Physics [17].

Meson Decay Mode	Branching Fraction (%)
$\pi^0 \to 2\gamma$	99
$\eta \to 2\gamma$	39
$\eta \to 3\pi^0$	33
$\eta \to \pi^+\pi^-\pi^0$	23
$\omega \to \pi^+\pi^-\pi^0$	89
$\omega \to \pi^0\gamma$	9
$\eta' \to \pi^+\pi^-\eta$	45
$\eta' \to \pi^0\pi^0\eta$	21
$\eta' \to 2\gamma$	2
$b_1(1235) \to \omega\pi$	dominant
$f_1(1285) \to \pi^0\pi^0\pi^+\pi^-$	22
$f_1(1285) \to \eta\pi\pi$	52
$a_2(1320) \to 3\pi$	70
$a_2(1320) \to \eta\pi$	15

Table 1.3: Neutral or charged + neutral decay modes of several well established mesons. Source: 2006 Review of Particle Physics [17].

1.2 Detector overview

To achieve the primary physics goal of GlueX, *i.e.* mapping out the spectrum of gluonic excitations, it is essential to detect charged partciles and photons with good acceptance and to measure their momentum, energies and positions with sufficient resolution. Charged particles include $\pi^{\pm}$, $K^{\pm}$ and protons, while the photons of particular interest are those resulting from $\pi^0 \to \gamma\gamma$ and $\eta \to \gamma\gamma$ decays. The GlueX detector, as shown in Figure 1.1, includes two tracking systems and two electromagnetic calorimeters to detect and measure these particles.

The GlueX detector is a solenoidal detector that is ideally suited for a fixed target photoproduction experiment. The solenoidal magnetic field traps low energy electromagnetic backgrounds (e^+e^- pairs), generated in the target, inside a small diameter beam hole that runs through the detector. The superconducting solenoid magnet produces a 2 T field. The photon beam is incident on a 30-cm LH_2 target that is surrounded by a cylindrical tracking chamber and a cylindrical electromagnetic calorimeter. Downstream of the target are circular planar tracking chambers and a circular planar electromagnetic calorimeter.

1.3 Information from existing photoproduction data

There is little data on meson photoproduction in the GlueX energy regime ($E_\gamma \approx 7 - 9$ GeV). Almost all of what is known comes from bubble chamber measurements at SLAC [18, 19, 20, 21, 22, 23]. These experiments were among the first exploratory studies of the photoproduction of meson and baryon resonances at these energies, and although they suffer from low-statistics, they have good acceptance, except for events with multiple neutrals. Exclusive reactions leading to final states with charged particles and a single neutron or π^0 can be identified by kinematic fitting. Table 1.4 summarizes the photoproduction cross sections for various charged particle topologies, with and without neutrals, at $E_\gamma = 9.3$ GeV [18]. Final states with single or multi-neutral particles (π^0, η or n) account for about 82% of the total cross section. About 13% of the total cross section is due to final states with charged particles and a single π^0. So for about 70% of the total photoproduction cross section, from $E_\gamma \approx 7$ to ≈ 12 GeV, we have essentially no information. Extrapolating from what is known from the final states that have been identified and studied, the bulk of the unknown processes are expected to involve final states with combinations of π^0 and η mesons. The discovery potential of GlueX rests on being able to detect π^0 and η mesons in addition to the charged particles.

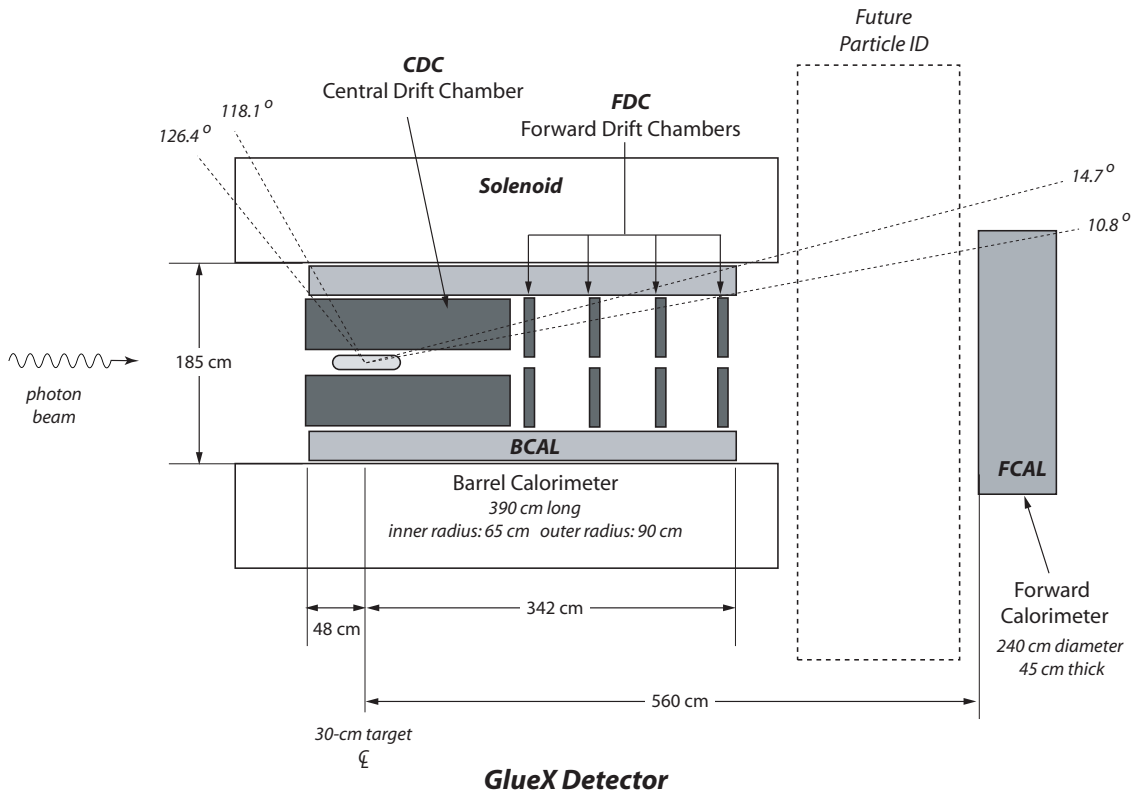

Figure 1.1: Schematic of the GlueX Detector. The superconducting solenoid magnet produces a 2 T field. The photon beam is incident on a 30-cm LH_2 target that is surrounded by a cylindrical tracking chamber (CDC) and a cylindrical electromagnetic calorimeter (BCAL). Downstream of the target are circular planar tracking chambers (FDC) and a circular planar electromagnetic calorimeter (FCAL). The dimensions of BCAL and FCAL are shown. The detector has cylindrical symmetry about the beam direction. The dashed lines at angles (with respect to the beam direction) 10.8° through 126.4° will be referenced in the text.

Baryon resonance decays: Photoproduction of meson resonances in the GlueX energy regime typically result in the meson being produced at small absolute values of the momentum transfer squared $|t|$ between incoming photon and outgoing meson – or equivalently between target proton and recoil nucleon or baryon resonance. The produced meson, as well as its decay products (depending on the particle multiplicity and relative mother-daughter masses), move in the forward direction whereas the recoil baryon moves at large angles $\gtrsim 45°$ with respect to the beam direction. If the recoil baryon is a baryon resonance, such as a Δ or N^*, decays involving π^0 are possible. It will be important to identify the soft, wide-angle π^0 mesons from such decays since the amplitude analysis depends on starting with a known exclusive reaction.

1.3.1 Studies using PYTHIA

As noted above, much is unknown about photoproduction at GlueX energies leading to multi-neutral final states. To estimate photon yields we used the Monte Carlo program PYTHIA [24] that was written to generate high energy physics events produced in a wide variety of initial states, including fixed target photoproduction. The program is based on a combination of analytical results and QCD-based models of particle interactions. PYTHIA was designed to allow for tuning parameters to suit the particular situation – for example, photoproduction at 9 GeV. The output of the simulations were compared [25] to published data, in particular, reference [18]. Comparison of cross section estimates for charged particle topologies and

Topology	σ (μb)	% of σ with neutrals
1-prong	8.5 ± 1.1	100
3-prong	64.1 ± 1.5	76 ± 3
5-prong	34.2 ± 0.9	86 ± 4
7-prong	6.8 ± 0.3	86 ± 6
9-prong	0.61 ± 0.08	87 ± 21
With visible strange decay	9.8 ± 0.4	-
Total	124.0 ± 2.5	82 ± 4

Table 1.4: Topological photoproduction cross sections for γp interactions at 9.3 GeV from Reference [18]. Also shown are the percent of the cross section with neutral particles for each topology.

several reactions in the 3-prong and 5-prong, which accounts for 80% of the total cross section, are shown in Tables 1.5 and 1.6. The vector mesons ρ, ω and ϕ appear in the 3-prong sample in the $\pi^+\pi^-p$, $\pi^+\pi^-\pi^0p$ and K^+K^-p final states respectively. The distribution in $|t|$ for PYTHIA events agrees with published data for specific reactions. PYTHIA accounts for Δ resonance production. In the $\pi^+\pi^-K^+K^-p$ state, the $K^*(890)$ is present.

Topology	PYTHIA Estimates (μb)	Data (μb)
1-prong	8.8 ± 0.02	8.5 ± 1.1
3-prong	63.5 ± 0.09	64.1 ± 1.5
5-prong	42.7 ± 0.2	34.2 ± 0.9
7-prong	7.3 ± 0.1	6.8 ± 0.3
9-prong	0.3 ± 0.1	0.61 ± 0.08

Table 1.5: Topological Photoproduction Cross Sections at 9 GeV from PYTHIA and from bubble chamber data [18]. The PYTHIA cross section estimates have been tuned to a total photoproduction cross section of 124 μb. The errors on the PYTHIA estimates are statistical.

1.4 Charged particle kinematics in GlueX

Charged particles ($\pi^\pm$, $K^\pm$ and p) will be reconstructed using two tracking systems. The CDC around the target and the FDC in the down-stream half of magnet. The CDC [7] is a 24-layer, 1.5m long straw tube chamber while the FDC [8] packages are cathode-plane drift chambers. These are described in detail later documents. Here we only cite that the CDC should achieve a 150 μm resolution normal to the wire. Using stereo layers, a z resolution along the wire of about $\sim$ 1.5mm can be achieved. The FDC will make measurements in the x-y plane (normal to the beam direction) with a resolution of 200 μm. Together, these detectors will track particles from threshold up to nearly 8 GeV/c. The kinematics of the photoproduction reaction tend to give the particles a forward boost with the highest momentum particles traveling at small angles and essentially detected only in the FDC. Particles with larger transverse momentum tend to have lower over all momentum and will be tracked in some combination of the two chambers.

Semi-quantitatively, particles going more forward than about 1° in the lab will go down the beamline and not be seen by any tracking detector. Outside of this to about 6°, particles will be seen only in the FDC. From 6° out to 30°, particles can be seen by both the CDC and the FDC. Realistically, for both the CDC and the FDC to be used in reconstruction, the particles are in the range of about 8° to 24°. From 30° to about 150°, particles can be reconstructed in the CDC, and hits will be seen in the CDC back to 168°, but resolution is likely to be poor due to there being fewer than 10 hits on a track.

The Forward Hole: More precisely, the forward hole in the GlueX acceptance has been defined by background rates in the FDC detectors. These background rates limit the size of the hole to about 1° in

Reaction	PYTHIA Estimates (μb)	Data (μb)
	$\gamma p \to 3$ prongs	
$\gamma p \to p\pi^+\pi^-$	13.6 ± 0.13	14.7 ± 0.6
$\gamma p \to pK^+K^-$	0.41 ± 0.02	0.58 ± 0.05
$\gamma p \to p\bar{p}p$	0.04 ± 0.01	0.09 ± 0.02
$\gamma p \to p\pi^+\pi^-\pi^0$	5.8 ± 0.1	7.5 ± 0.8
$\gamma p \to n2\pi^+\pi^-$	1.4 ± 0.04	3.2 ± 0.7
With multi-neutrals	42.3 ± 0.3	38.0 ± 1.9
	$\gamma p \to 5$ prongs	
$\gamma p \to p2\pi^+2\pi^-$	2.9 ± 0.06	4.1 ± 0.2
$\gamma p \to pK^+K^-\pi^+\pi^-$	0.51 ± 0.03	0.46 ± 0.08
$\gamma p \to p2\pi^+2\pi^-\pi^0$	8.12 ± 0.1	6.7 ± 1.0
$\gamma p \to n3\pi^+2\pi^-$	$0.8 \pm .3$	1.8 ± 1.9
With multi-neutrals	30.4 ± 0.2	21.1 ± 1.7

Table 1.6: Photoproduction reaction cross sections at 9 GeV from PYTHIA and from bubble chamber data [18]. The PYTHIA cross section estimates have been tuned to a total photoproduction cross section of 124 μb. The errors on the PYTHIA estimates are statistical.

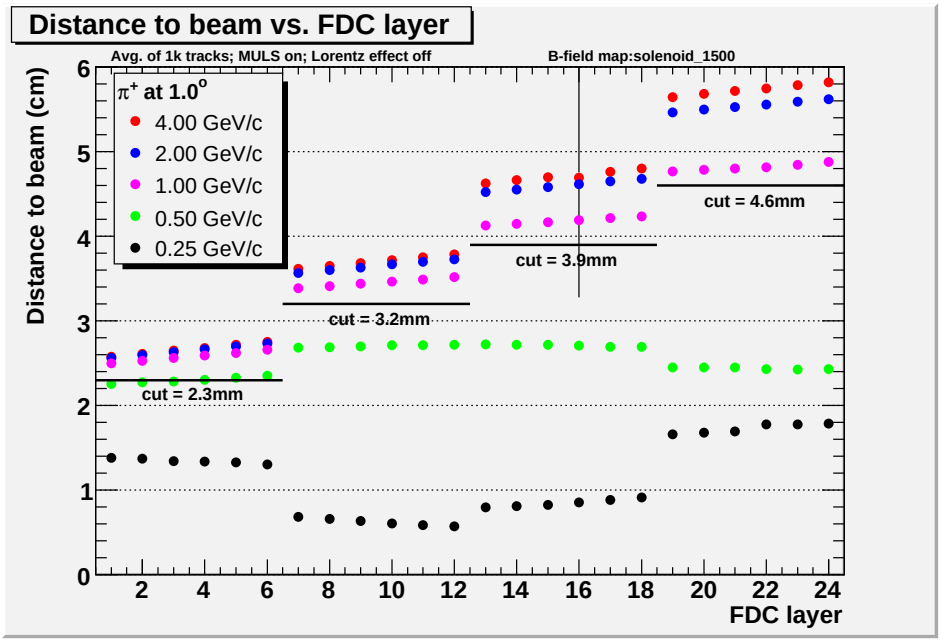

Figure 1.2: The forward hole near the beamline in the FDC is defined by the requirement that $1\,GeV/c$ π^+ with $\theta = 1°$ will be measured in the FDC. The plots shows the maximum size of the hole around the beamline in each FDC package for various values of the π^+ momentum at 1°. The odd structure for $0.5\,GeV/c$ and $0.25\,GeV/c$ particles occurs due to spiraling of the tracks in the solenoidal field.

polar angle (θ). To make the hole uniform in all four FDC packages, the hole is defined by tracking 1GeV/c π^+ through the detector and measuring the distance from the beam line in each of the four FDC packages. The result of this is shown in Figure 1.2. In particular, the first FDC package has a hole that is 2.3mm in radius and the fourth package has a hole that is 4.6mm in radius.

As can be seen in Figure 1.2, the angular size of the forward hole becomes somewhat smaller as momentum is increased above 1GeV/c and is larger for lower momenta. In particular, the curves which correspond to

0.25GeV/c and 0.5GeV/c show what appears to be an odd structure in the Figure. In fact, it is just the particles spiraling in the magnetic field as they move through the detector. Particles with 0.25GeV/c momentum are on the innermost part of a spiralling loop in FDC packages two and three. Because of spiraling of these low momentum particles, it does not make a great deal of sense to use them in defining the size of the forward hole.

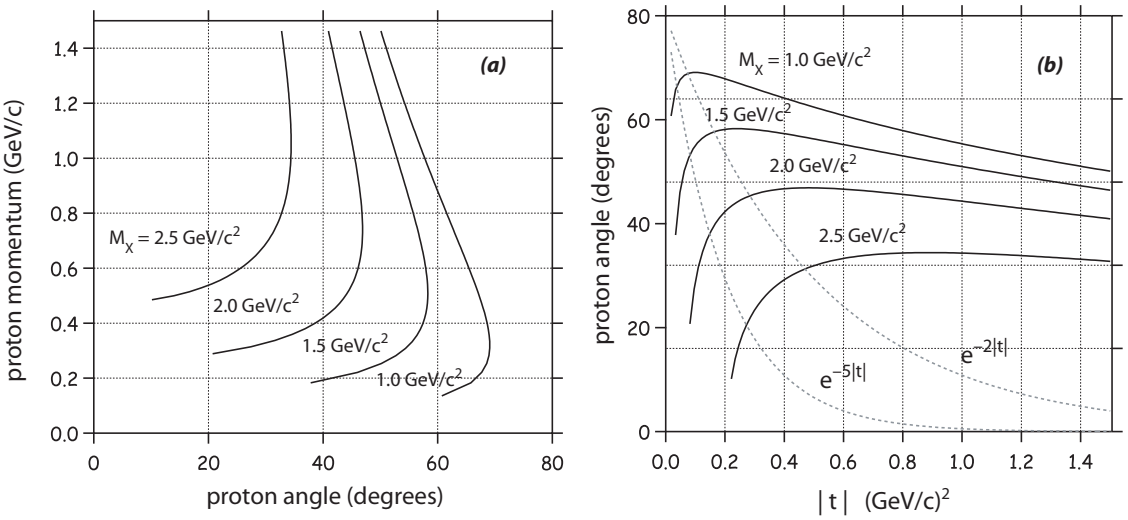

Figure 1.3: (a) Recoil proton LAB momentum as a function of proton LAB angle, measured with respect to the beam direction, for $\mid t \mid_{min} < 1.5\,(GeV/c)^2$ for the reaction $\gamma p \rightarrow Xp$ for $M_X = 1.0, 1.5, 2.0$ and $2.5\,GeV/c^2$. (b) Recoil proton LAB angle, measured with respect to the beam direction as a function of $\mid t \mid$ for the reaction $\gamma p \rightarrow Xp$ for $M_X = 1.0, 1.5, 2.0$ and $2.5\,GeV/c^2$. Also shown are typical t distributions for $e^{-2|t|}$ and $e^{-5|t|}$ (light dotted curves).

Reactions of Interest for Hybrid Mesons: In order to understand how particles of various momentum populate the tracking elements, we need to consider some typical reactions which are part of the GlueX physics program. The first of these is the generic reaction $\gamma p \rightarrow pX$, where X represents a mesonic system whose mass can go up to around $2.5\,GeV/c^2$. Such a reaction is expected to be produced in a t-channel process where the cross section has an exponential dependence on the magnitude of t, $e^{-\alpha|t|}$, with the slope, α varying from 2 to 5. Such a reaction defines the proton kinematics in the GlueX detector. Figure 1.3 shows the lab momentum and angles for protons produced in the reaction $\gamma p \rightarrow pX$ with X varying in mass from 1.0 up to $2.5\,GeV/c^2$. Virtually all of these protons are seen in the forward half of the CDC, with many of them also seen in the FDC packages. For $m_X = 2.5\,GeV/c^2$, the most forward protons have a total momentum of about $0.4\,GeV/c$ with this momentum becoming smaller as the mass of X gets smaller.

A signature reaction for GlueX is $\gamma p \rightarrow n\pi^+\pi^+\pi^-$, where the 3π system has a mass in the range of 1.5 to $2.5\,GeV/c^2$. The distributions of charged pions from this reaction shown in Figure 1.4. About 50 % of these pions are only seen in the FDC. Most of the remainder are seen in both the CDC and FDC with a tail of particles below about $1.5\,GeV/c$ seen only in the CDC. Other important reactions have larger numbers of pions, (4, 5, 6, $\cdots$). As the final state multiplicity becomes larger, the average particle momentum gets smaller, and slower particles are seen at larger angles in the CDC. For the reactions of interest for amplitude analysis in GlueX, the detector acceptance very good for all of these reactions.

The hybrid strangonium states are expected to decay predominantly through several final states which eventually populate the reaction $\gamma p \rightarrow pK^+K^-\pi\pi$. Within this final state, the following reactions are

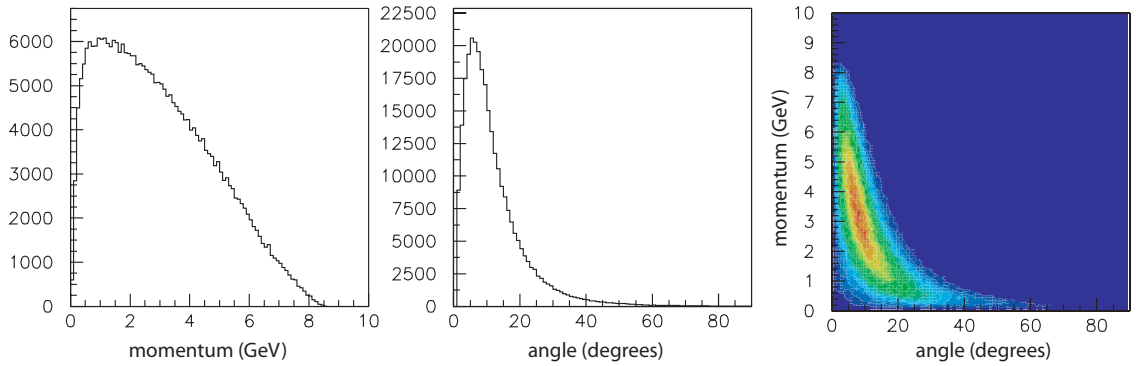

Figure 1.4: The momentum and angle spectra of charged pions and their correlation from the reaction $\gamma p \rightarrow \pi^+\pi^+\pi^-n$ for 8.5 to 9.0 GeV photons.

predicted by decay models to be the dominant decay modes.

$$\begin{aligned} \gamma p &\rightarrow K_1^{\pm}(1410)K^{\mp} \\ \gamma p &\rightarrow K_1^{\pm}(1270)K^{\mp} \\ \gamma p &\rightarrow K^*(892)\bar{K}^*(892) \\ \gamma p &\rightarrow \phi(1020)f_0(980) \end{aligned}$$

Assuming t-channel production, the distribution of kaon momentum versus angle are shown in Figure 1.5 for the four reactions above, where one assume a t slope of $\alpha = 5$ and a hybrid mass in the range of 2 to 2.5 GeV/c^2—in line with all current hybrid predictions. These kaons tend to populate both the FDC and the forward part of the CDC and have momenta from several hundred MeV/c up to nearly 6 GeV/c, with the highest momentum tending to be in the very forward direction. In terms of reconstructing the charged particles, this is a very good match to the GlueX tracking systems.

All of the reactions examined above tend to populate the GlueX tracking system with angles well forward of 90° in the lab. This is true for t-channel processes where a neutron or proton is connected to the lower vertex—the expected hybrid production mechanism. However, a competing reaction ($\gamma p \rightarrow \Delta X$) can generate both charged and neutral pions at more backwards angles. In this case, the pion from the decay of the Δ can by sent into the backwards direction. For charged particles, the acceptance of GlueX is still very good for these relatively slow pions.

Low Momentum Cutoffs: Monte Carlo studies have been carried out to quantify the the low-momentum thresholds for charged particles in GlueX. These cutoffs are dominated by energy loss in material before reaching the tracking volumes as well as bending in the strong magnetic field. If we consider particles that are nominally seen by the CDC, the cutoff as a function of polar angle from 15° to 90° in the lab and momentum is shown in Figure 1.6. Pions with momenta smaller than about 0.15 GeV/c cannot be reconstructed in GlueX . For kaons, the cutoff is similar to pions at large angles, but rises to about 0.22GeV/c for forward going Ks. Protons have a more difficult time with the cut off falling from about 0.33GeV/c in forward directions down to about 0.25GeV/c at 90° in the lab. In terms of overall reconstruction, the missing proton produces the largest hole in the GlueX acceptant. Combining this cut off with the information in Figure 1.3, we see that for mesons systems (X) with masses below about 2 GeV/c^2, the low-t production will tend to produce a proton that will not be easily detected in GlueX . These protons will have to be reconstructed using kinematic fitting and missing mass techniques.

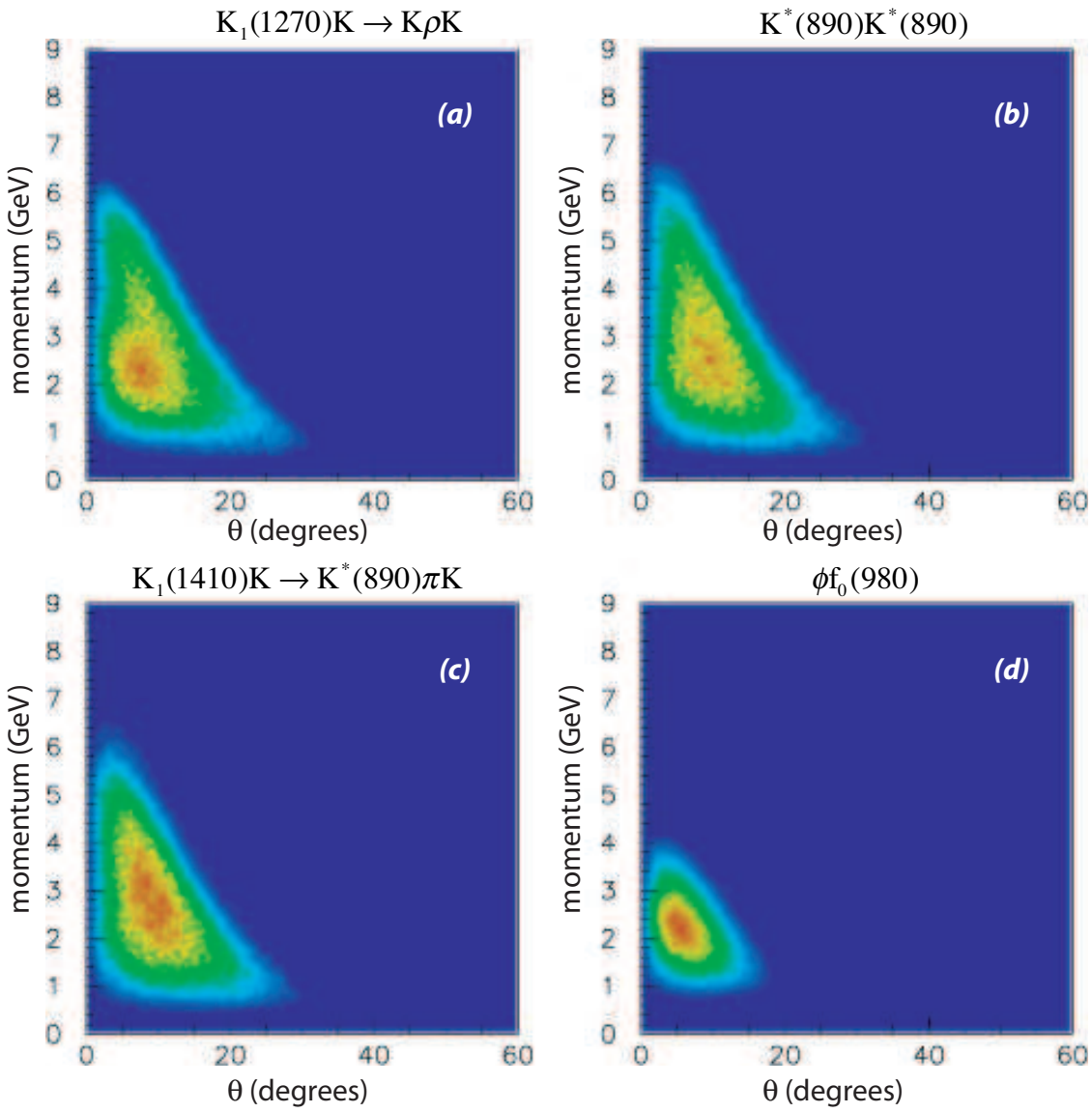

Figure 1.5: The momentum versus angle (in the lab) for $K^{\pm}$ in the reaction $\gamma p \to pK^+K^-\pi\pi$ for various intermediate states. (a) $K_1^{\pm}(1270)K^{\mp}p$; (b) $K^*(890)\bar{K}^*(890)$; (c) $K_1^{\pm}(1410)K^{\mp}p$; and (d) $\phi(1020)f_0(980)$.

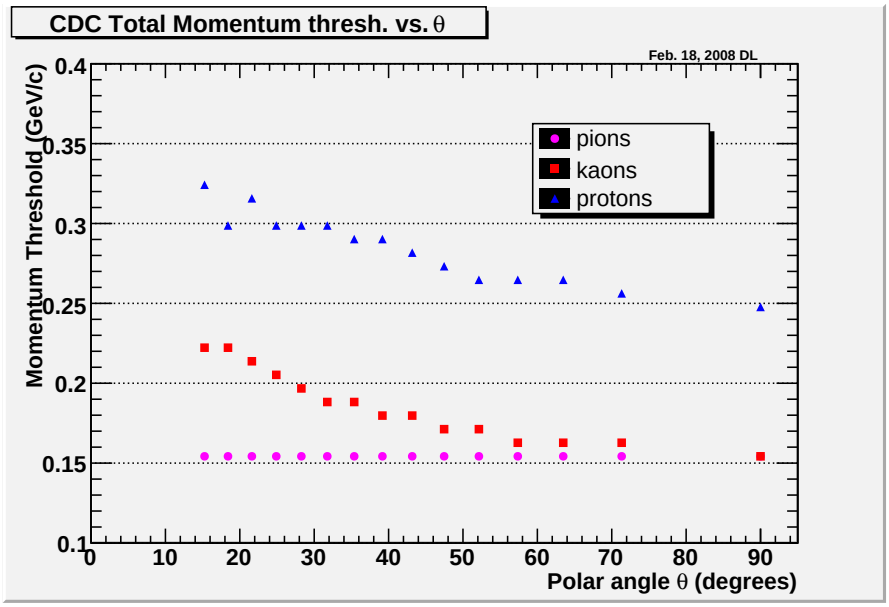

Figure 1.6: Momentum threshold for reconstructing charged particles in the CDC.

1.5 Momentum resolution and reconstruction efficiencies for charged particles

As discussed in section 1.4, charged particles are tracked through the detector using the CDC and FDC chambers. The CDC measures position normal to a wire to accuracy of about 150μm and through the use of $\pm 6^\circ$ stereo layers, can determine the position along the beam direction to an accuracy of about 1.5mm. The FDC measures positions of hits in the plane normal to the beam direction to an accuracy of about 200 μm, while the position in z is defined by how well the location and relative orientation of the chamber packages is known.

To determine the momentum resolution for charged particles in GlueX, the particles are tracked through the detector simulation (HDGeant [31],[32] using GEANT 3.14). This simulation contains our best estimates of all the material in GlueX as well as models for all relevant detector responses. The resulting events are then reconstructed using the GlueX reconstruction software [33]. The current software uses hits from the chambers with design resolutions to find and then fit the tracks. Both the Monte Carlo and the reconstruction software use a realistic field map for the solenoidal magnetic field including fringe fields out to the time-of-fligh wall.

To obtain the momentum resolution of GlueX, charged particles of a given momentum, $\vec{p}$, are generated and tracked through the detector. The fit momentum is then compared with the generated momentum. This leads to the resolution plots shown in this section. These studies map out the resolution of the detectors independent of the probability of the underlying physics producing such an event. In particular, there are large regions of the mapped resolution where there will be no physics events.

We start with the momentum resolution,

$$\sigma_{\Delta p/p} \quad = \quad \frac{\Delta \mid \vec{p} \mid}{\mid \vec{p} \mid} .$$

Figure 1.7 shows a scatter plot of $\sigma_{\Delta p/p}$ as a function of $\mid \vec{p} \mid$ (vertical axis) and polar angle θ (horizontal axis). Most of the plot shows a momentum resolution on the order of 1 to 2 %. Figure 1.8 shows a projection of 1.7 for several fixed values of total momentum in the range of 1 to 7 GeV/c. There are several structures in 1.8 which can be understood in terms of the geometry of the detector. The degradation in resolution for very forward tracks is due to the little measured bending for these tracks which go roughly parallel to the magnetic field in GlueX . The bumps that occur on the 10° to 25° range correspond to particles not hitting all the FDC packages. A jump is observed each time a package is not hit. The rise in the backwards direction corresponds to particles missing the CDC—however this structure is in regions of phase space which have no events. In fact, most of the angular region beyond 40° will rarely see particles of momentum larger than 2 GeV/c. Most particles in this region will have a momentum resolution better than 1.5%.

We next look at the polar angle resolution,

$$\sigma_{\Delta\theta} \quad = \quad \Delta\theta .$$

Figure 1.9 is a scatter plot showing $\sigma_{\Delta\theta}$ in milliradians as a function of both $\mid \vec{p} \mid$ (vertical axis) and polar angle θ (horizontal axis. Figure 1.10 is a projection of the angular resolution for slices of polar angle θ going from 10° to 90°. Finally, the azimuthal angular resolution

$$\sigma_{\Delta\phi} \quad = \quad \Delta\phi .$$

is shown in Figures 1.11 and 1.12.

Track Finding: The current version of the GlueX reconstruction software starts with a track-finding package that looks for tracks in the CDC and FDC separately, and then tries to merge them. Figure 1.13 shows the track-finding efficiency for this package as a function of both total number of hits and which chambers the tracks are located. A track is considered found if the identified hits look reasonably similar to the generated track. The solid triangles show the track finding efficiency when only the FDC is used as a function of the polar angle θ while the solid squares show the same plot for the CDC. The solid circles show

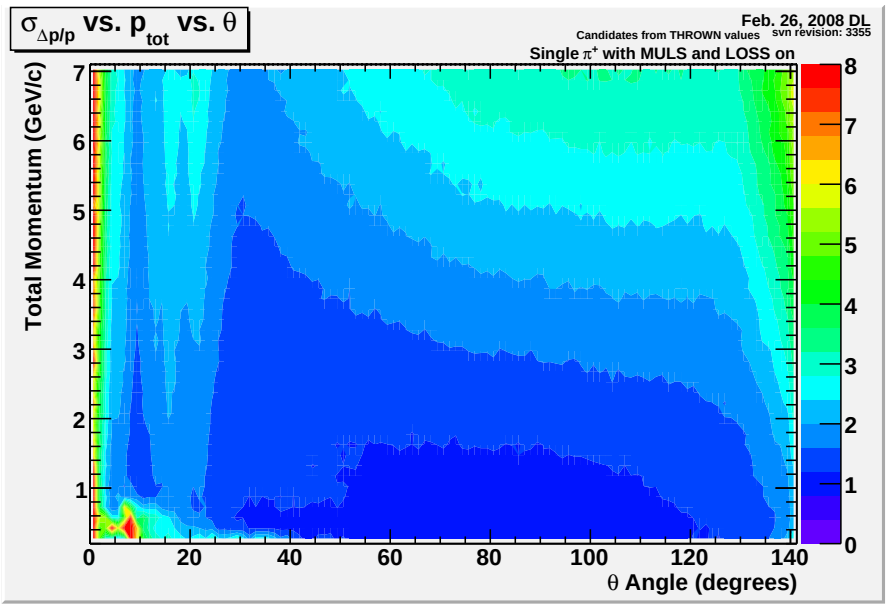

Figure 1.7: Total momentum resolution (%) as a function of the total momentum p and polar angle θ at the primary vertex.

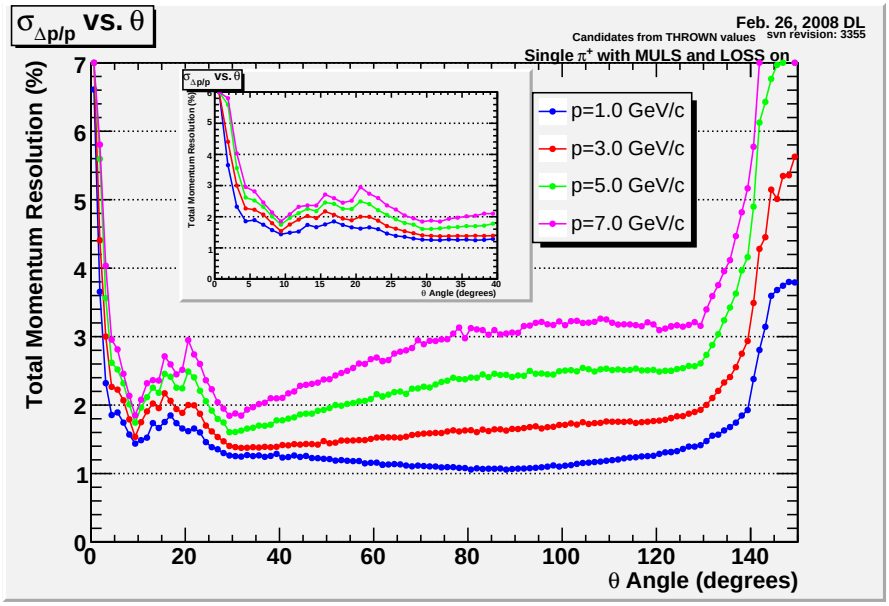

Figure 1.8: Total momentum resolution (%) as a function of the polar angle θ at the primary vertex for several values of momentum p. This plot is a projection of data in the scatter plot in Figure 1.7.

the efficiency for finding either a CDC or and FDC track. The colored regions labeled FDC and CDC map the number of hits on the track in the particular detector. Overall, there is good track-finding efficiency in GlueX. Nearly 100% efficiency except for a small transition region near 12°. It is expected that as the track finding software continues to develop over the next five years that these efficiencies will improve. Track-

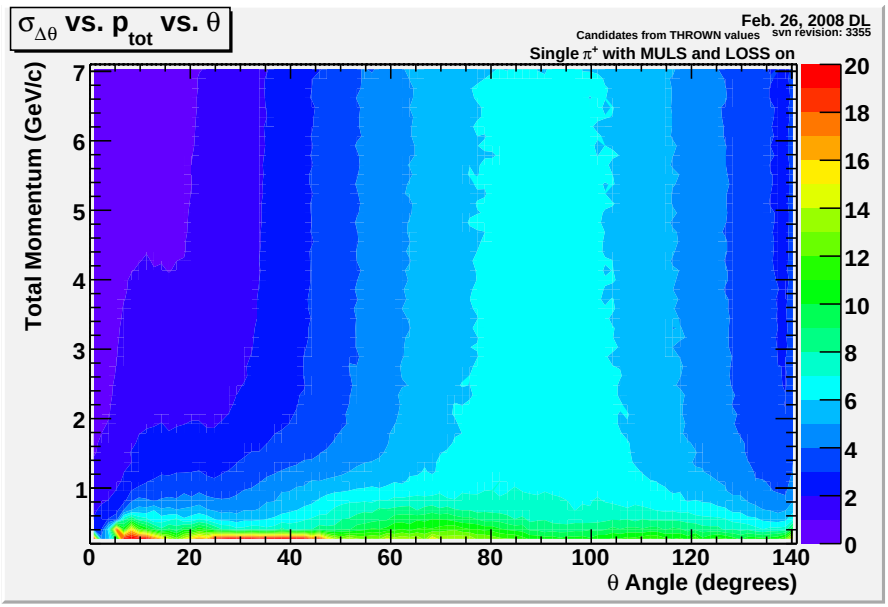

Figure 1.9: Polar angle resolution (mrad) as a function of the total momentum p for various polar angle θ at the primary vertex.

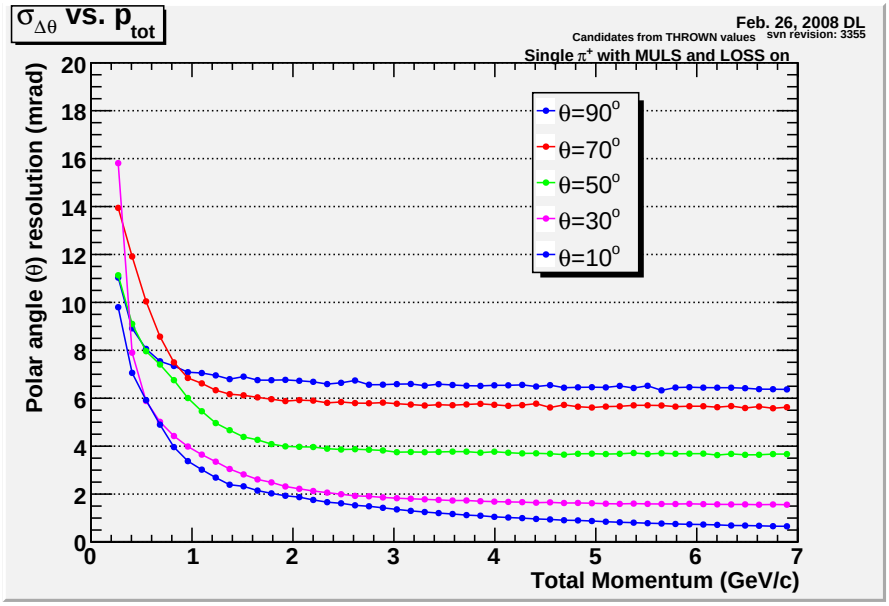

Figure 1.10: Polar angle resolution (mrad) as a function of the total momentum p for various polar angle θ at the primary vertex. This is a projection of Figure 1.9

finding in the presence of electromagnetic backgrounds have also been studied in GlueX.These studies show a small, few percent, degradation of the efficiencies (See Figure 1.13).

After carrying out track finding, the tracks need to be fit to obtain particle information. A track fitting package has been developed, but as with track finding, developmental improvements will continue over the

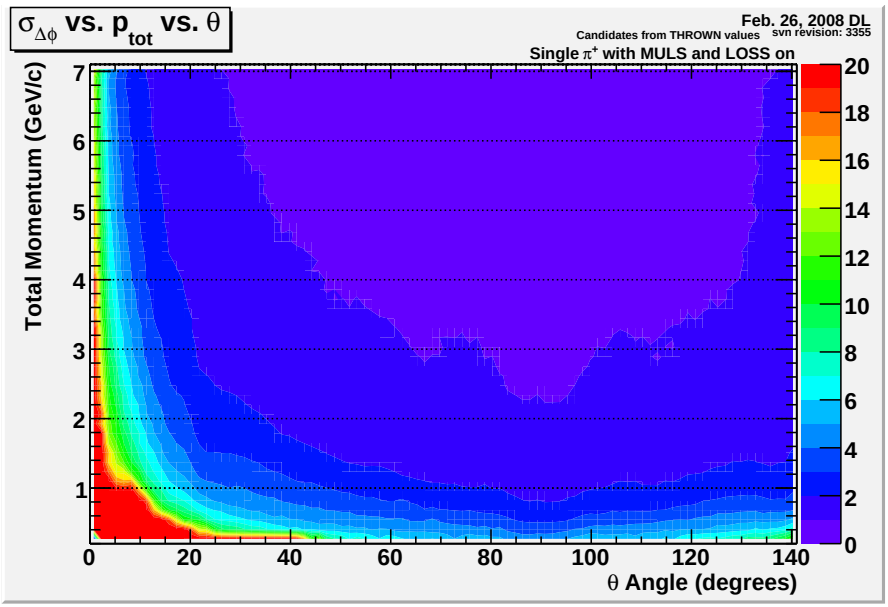

Figure 1.11: Azimuthal angle resolution (mrad) as a function of the total momentum p for various polar angle θ at the primary vertex.

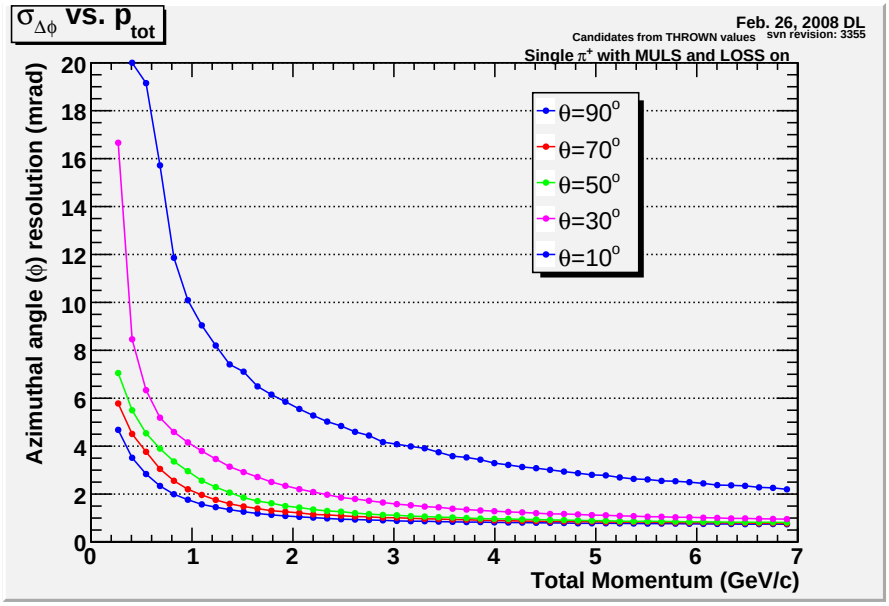

Figure 1.12: Polar angle resolution (mrad) as a function of the total momentum p for various polar angle θ at the primary vertex. This is a projection of Figure 1.11

next five years. At present, the GlueX track fitter is able to fit nearly 85% of the found tracks. The current 15% loss appears to be related to pathologies in the fitting routines. Work on resolving these deficiencies is in progess, and it is anticipate that the GlueX track fitting efficiency will improve and match that of the track finding.

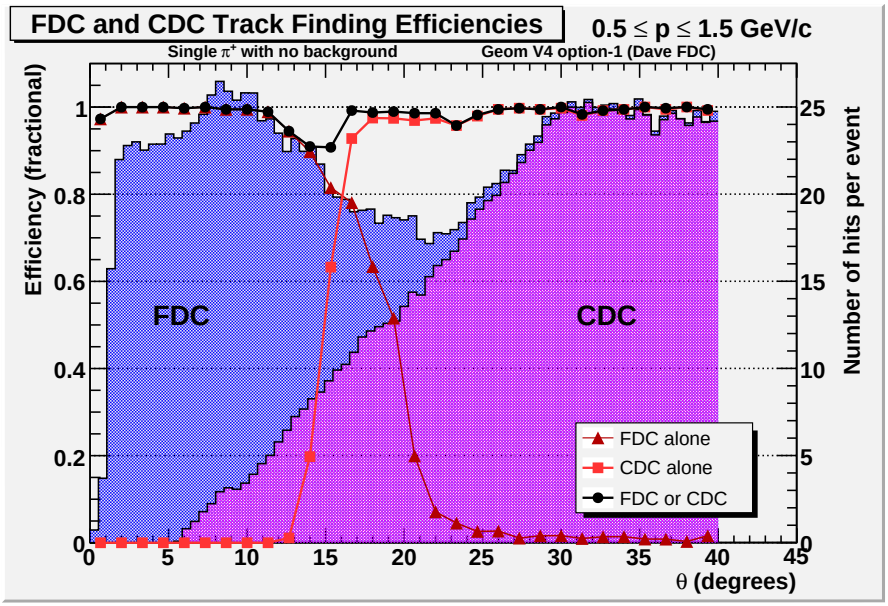

Figure 1.13: Track finding efficiency in the CDC and FDC, see text for explanation.

Parameterized Resolutions: Based on the resolutions obtained from HDGEANT and the GlueX reconstruction software, a set of parametrized resolution and acceptance functions have been developed. These functions provide a pseudo event reconstruction which can be used to carry out more sophisticated GlueX studies. An example of these studies are effective & missing mass studies and PWA amplitude analysis studies.

1.6 Mass resolutions involving charged particles and photons

To compare the contributions of charged particle resolution and photon resolutions to narrow width particles, as in the decays $\eta \to \pi^+\pi^-\pi^0$, $\omega \to \pi^+\pi^-\pi^0$ and $\phi \to \pi^+\pi^-\pi^0$ we studied the reaction $\gamma p \to \phi p$. For this study, the distribution in $|t|$ followed $e^{-|t|/2}$ to provide a mix of charged particle momenta that would include more lower momentum particles. The ϕ was generated with a mass and width of 1020 and 4 MeV/c^2 respectively. The photon energies and angles were smeared according to the nominal resolutions discussed above. The charged particle four vectors (for the $\pi^\pm$) were smeared to follow the momentum error and angular error plots generated in a study of track finding in GlueX [33]. The plots shown in the referenced study were fit to analytical forms. These plots were generated before the material associated with the CDC and FDC tracking chambers was reduced so in what follows we consider the nominal charged particle resolutions and resolutions improved by a factor of two. The effect of the resolution smearing on the observed width of the ϕ is shown in Table 1.7. The distribution in the square of the missing mass recoiling against the ϕ is shown in Figure 1.14 under various assumptions of four-vector smearing.

Condition	Nominal errors for $\pi^\pm$	Nominal errors/2 for $\pi^\pm$
Photon smearing only	14.8 ± 0.1 MeV/c^2	14.8 ± 0.1 MeV/c^2
Charged particle smearing only	16.7 ± 0.1 MeV/c^2	11.1 ± 0.1 MeV/c^2
Both smeared	22.2 ± 0.2 MeV/c^2	17.6 ± 0.1 MeV/c^2

Table 1.7: Observed width for the ϕ, generated with a width of 4 MeV/c^2, after four-vector smearing.

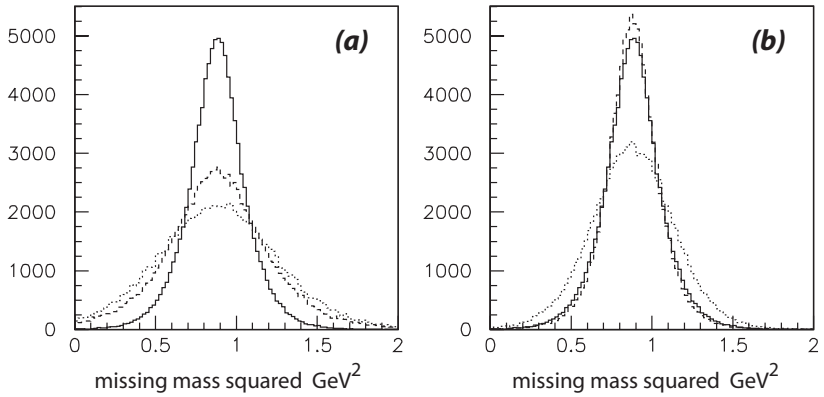

Figure 1.14: Missing mass squared recoiling off the ϕ for the reaction $\gamma p \to \phi p$ with photon smearing only (solid histogram), charged particle smearing only (dashed) and both (light dashed) for nominal charged particle smearing (a) and smearing reduced by a factor of two (b).

1.7 Particle Identification in GlueX

Separation of pions, kaons, protons and possibly electrons will be necessary to carry out the entire GlueX physics program. In order to do this, a comprehensive system of particle identification and analysis will be needed. In GlueX , this system will be staged in two parts—the first as part of the base-line detector and the second as an additional detector system that would come on line at a later time. As with most particle identification systems, these are somewhat redundant with each other. In addition to the hardware, we also anticipate sophisticated analysis that will look globally at an individual event to identify the best possible particle assignments consistent with all information.

In GlueX , the base-line hardware systems consist of a time-of-flight wall just in front of the FCAL which will measure times with a 70 ps accuracy and will see charged particles in a roughly 11° degree wide cone

about the beam axis. Additional information will come from timing measurements in the BCAL and possibly energy deposition from charged particles in the BCAL. Finally, the CDC will measure dE/dx information that will be useful for particles below $0.45\,GeV/c$ momentum.

The upgrade option for GlueX is a ring imaging Cerenkov counter (RICH) located in front of the time-of-flight wall. Such a detector would allow excellent particle identification for particles with momentum up to about $6\,GeV/c$. Space has been left in the detector design for this upgrade.

1.7.1 Time of flight information

As noted above, information about the time difference between the two ends of the BCAL module photosensor readout provides the impact point (z-position) of photons striking the inner surface of BCAL. The average time, or mean time, of the two ends can be used to provide time of flight information that may be used for particle identification. The time difference is relevant and crucial for determining the four-vector information for photons.

The mean time information could, in principle, be used for particle identification for hadrons, in particular in providing π/K or π/p separation. As will be discussed in what follows, the mean time resolution obtained from cosmic ray (minimum ionizing particle) measurements with a 4 m module, is approximately 500 ps. This time resolution is inadequate for π/K separation but can be used for π/p separation.

We generated events to simulate the reaction $\gamma p \rightarrow \pi^+\pi^-\pi^0 n$ where the 3π result from the decay $a_2(1320) \rightarrow \rho\pi$ or $\pi_2(1320) \rightarrow f_2\pi$ with a $e^{-5\cdot|t|}$. The charged particles were tracked through a uniform magnetic field and for $\pi^\pm$ reaching BCAL the π/K difference was computed. The time difference distribution is shown in Figure 1.15(a). Clearly, a 500 ps mean-time resolution does not allow for π/K separation. For protons reaching BCAL, we compute the π/p time difference divided by 500 ps. The resulting distribution is shown in Figure 1.15(b). About 77% of the events where the proton track has sufficient transverse momentum to reach BCAL have a $(t_p - t_\pi)/\sigma_t > 4$.

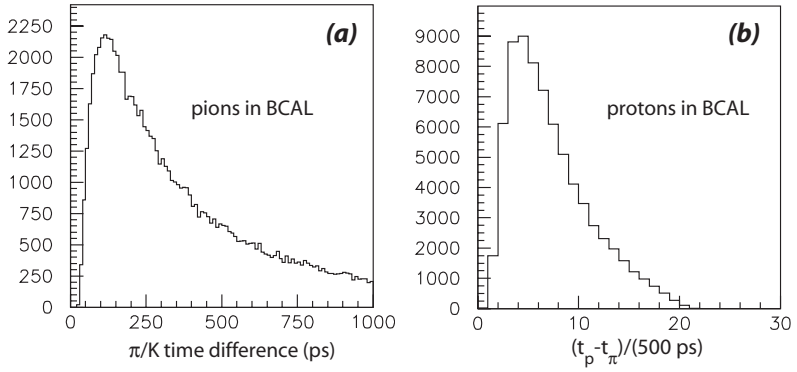

Figure 1.15: (a) The distribution in π/K time difference for $\pi^\pm$ reaching BCAL from the reaction $\gamma p \rightarrow \pi^+\pi^+\pi^- p$; (b) For protons reaching BCAL, the proton/pion time difference divided by 500 ps, the assumed mean time resolution for BCAL for minimum ionizing particles.

1.7.2 dE/dx in the CDC

The CDC will provide dE/dx information for charged particles. Given the fact that the path length in a straw is not a constant, this is more difficult than in a conventional drift chamber, however, it has been done [34]. For GlueX, the particles of interest have total momentum less than 0.45GeV/c, and are thus unlikely to be seen in any other particle identification system. Several studies have been done to look at the energy deposition in the straws from pions, kaons and protons. The results of these are summarized in

Figure 1.16. The left-hand plot shows particles moving at a polar angle of 90° in GlueX. For such particles, those with total momentum less than 0.25GeV/c will spiral and miss the BCAL. We also note that while none of the protons with momentum so low will be detected (see Figure 1.6), higher momentum protons will be slowed down to fall into this momentum range. For such particles, there is very good separation between all three particle species.

The right-hand plot in Figure 1.16 shows the same dE/dx calculation for particles moving forward at 15°. Here we consider particles lower than 0.45GeV/c and we see that while the π-K separation may be difficult, we should be able to carry out excellenr π-p separation.

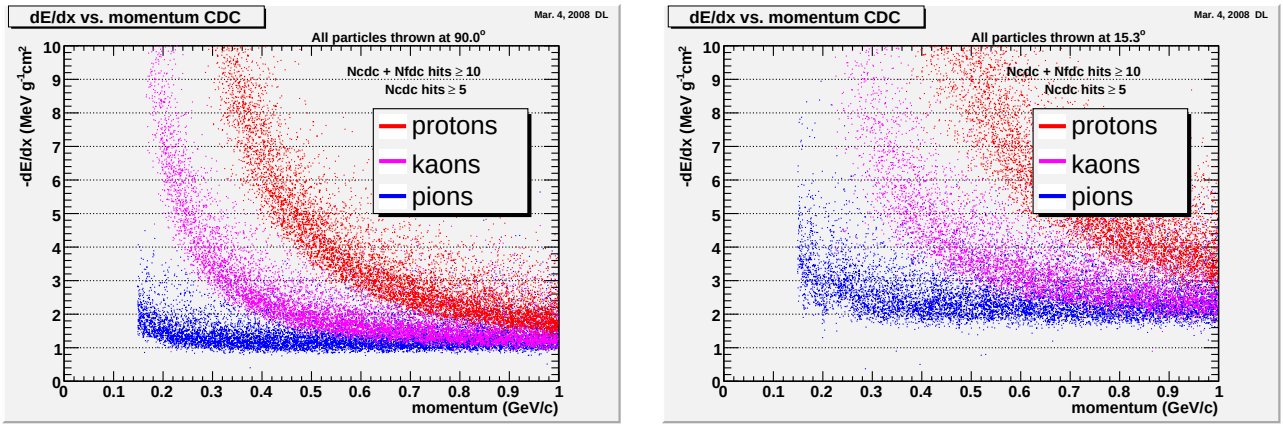

Figure 1.16: Expected energy loss as a function of particle momentum in the CDC, taking into account of the path length in each CDC straw. (left) Tracks going at 90° in the lab. (right) Tracks going at 15° in the lab. Very good π-p separation is seen for track momentum below $0.5\,GeV/s$, while less significant π-K separation will be possible.

1.7.3 Global Event Analysis

Individual particle identification systems provide a most probable assignment to for particle type based on information in a single detector. Physics principles such as strangeness conservation in conjunction with analysis tools such as kinematic fitting can be used to make global particle assignments to all particles in an event. Studies carried out with realistic resolutions in GlueX in conjunction with kinematic fitting have been carried out [35]. This looks at the following two reactions in GlueX to deterine what can be done with global fitting.

$$\begin{aligned} \gamma p &\rightarrow p K^+ K^- \pi^+ \pi^- \\ \gamma p &\rightarrow p \pi^+ \pi^- \pi^+ \pi^- \end{aligned}$$

The first is a signature reaction, while the second is a fairly prolific final state in GlueX. The two were generated in ratio of 1 in 100 which roughly follows the known cross sections. The studies also included intermediate resonances in various two-meson sub systems.

When no particle identification is assumed, there are 15 ways to make particle assignments in the final state. With a positive cut at 10% confidence level on the correct hypothis and a rejection of the wrong hypothesis at the 10% confidence level, we find that about 45% of the true signal survive and 1% of second reaction survives. This leades to a spectrum that has about twice as much background as true signal. If we then extend this study to include the situation where the proton has been positively identified in one of the GlueX syetems, the combinatorics falls from 15 to 5 and the amount of background leaking through goes down by another order of magnitude with the accepted background now representing about 8% of the accpeted signal. However, this requires that we reject roughly 55% of the true signals.

As we continue this by including a probabalistic time-of-flight measurement, the acceptance for true signal goes up and the background rejection conyinues to improve.

1.8 Expectations for amplitude analyses

The ultimate goal of the GlueX experiment is to identify exotic mesons by an amplitude analysis of exclusive final states. The sensitivity of the amplitude analysis, *i.e.* how small a signal can be detected, depends on having sufficient statistics and how well systematics, both from the experiment and from the analysis, are controlled. GlueX collaborators have recently been awarded an NSF grant to develop tools for understanding the phenomenological systematics inherent in an amplitude analysis. To estimate the sensitivity we expect from GlueX requires a full simulation of the detector response to real and background events, charged particle and photon reconstruction, kinematic fitting to identify exclusive final states and finally the actual amplitude analysis. Work is in progress and the last section of this report summarizes results from the first steps along this program.

There is a substantial literature on the decay of exotic mesons decaying to 3π final states with the most recent analysis of Brookhaven E852 data presented in reference [38]. While the existence of an exotic state at a mass of $1.6\,GeV/c^2$ which decays to three pions is somewhat in question, the partial wave analysis carried out in that reference stands as a benchmark as to what can be done. Figure 1.17 shows the results of the amplitude analysis for the $J^{PC} = 2^{++}$ and $J^{PC} = 4^{++}\rho\pi$ amplitudes. Two well-established meson states are observed in these amplitudes, the tensor state $a_2(1320)$ in the former and the spin-4 state $a_4(2040)$ in the latter. The intensity of the a_4 is about 3% that of the a_2 and the amplitude of the a_4 is similar for the $\pi^-\pi^0\pi^0$ and $\pi^-\pi^-\pi^+$ systems, even though the experimental systematics for these two modes are very different.

It is reasonable to ask how well the GlueX sensitivity will compare to E852. The resolutions obtained for the π^0 and η mass resolutions for GlueX calorimetry are similar to those obtained in E852. Studies are underway to estimate the charged particle momentum and angle resolutions by using current best-estimate resolution and acceptance functions. In this comparison, we have found that the widths of narrow resonances reconstructed in E852 and those in GlueX are quite similar, with the GlueX typically having somewhat narrower widths. Overall, we find that with the design resolutions of GlueX ,we are able to reconstruct things at least as well as was carried out in E852, and thus we should be able to carry out an amplitude analysis with at least the same level of precision.

1.8.1 A signature reaction: $\gamma p \to 3\pi p$

The $\pi^-\pi^-\pi^+$ and $\pi^-\pi^+$ effective mass distributions and distribution in momentum transfer from incoming beam to outgoing 3π system observed in E852 were used to generate a Monte Carlo event sample of a similar final state for 9 GeV photoproduction. Figure 1.18 shows various distributions from the three pion system. In the right-hand plots are distributions for E852 using an $18\,GeV/c$ π^- beam to examine $\pi^-p \to \pi^-\pi^-\pi^+p$. The left-hand plots show the simulated GlueX data of the reaction $\gamma p \to n\pi^+\pi^+\pi^-$ for 8.5 to $9.0\,GeV$ photons. For the case of GlueX only a finite number of t-channel produced resonances were included. In looking at the plots, the overall distributions look quite similar, and while what are seen are not particularly narrow resonances, the structures look very much the same.

Missing mass resolution: Since, for both the GlueX simulation and E852, information about the nucleon recoiling against the 3π system is not used in kinematically identifying the event, the comparison is of interest. Note that for the E852 case, the beam energy was a factor of two higher and the magnetic spectrometer was based on dipole magnet that produced a nearly uniform 1 T magnetic field over a volume that was 1.8 m wide (in the bend plane), 1.2 m high and 4.6 m long (along the beam line). The missing mass squared distribution for the GlueX Monte Carlo sample is shown in Figure 1.19 along with a Gaussian fit (solid line). The σ for the Gaussian fit is 0.27 $(\mathrm{GeV}/c^2)^2$. The corresponding E852 missing mass squared distribution had a σ of 0.31 $(\mathrm{GeV}/c^2)^2$[38].

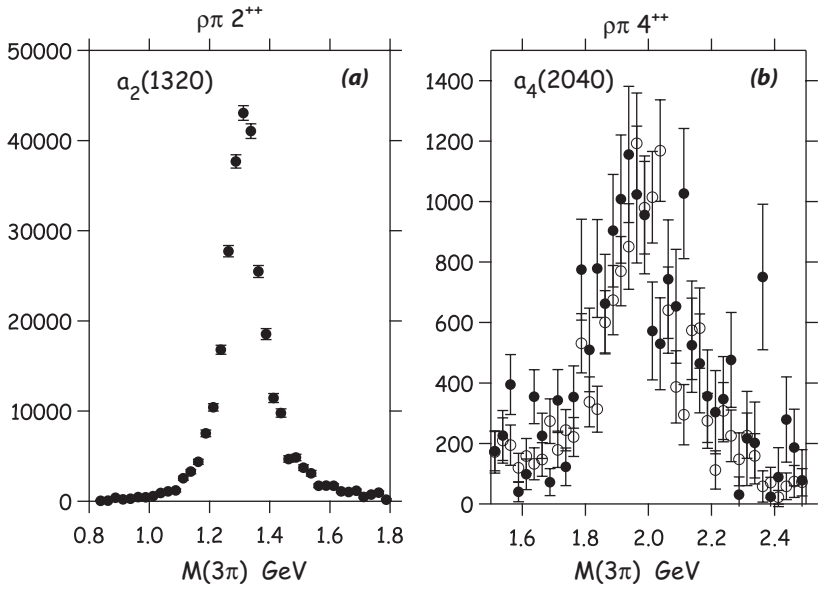

Figure 1.17: (a) Results of an amplitude analysis of data from $\pi^- p$ interactions at 18 GeV/c leading to the final states $\pi^-\pi^0\pi^0 p$ and $\pi^-\pi^-\pi^+ p$ from Brookhaven experiment E852 [38]. Results are shown for the (a) $J^{PC} = 2^{++}$ and (b) $J^{PC} = 4^{++}\rho\pi$ amplitudes. Filled circles are for the $\pi^-\pi^0\pi^0$ system and unfilled for the $\pi^-\pi^-\pi^+$ system. In (a) the tensor state $a_2(1320)$ is observed and in (b) the well-established spin-4 $a_4(2040)$ is seen. Note that the intensity of the a_4 is about 3% that of the a_2.

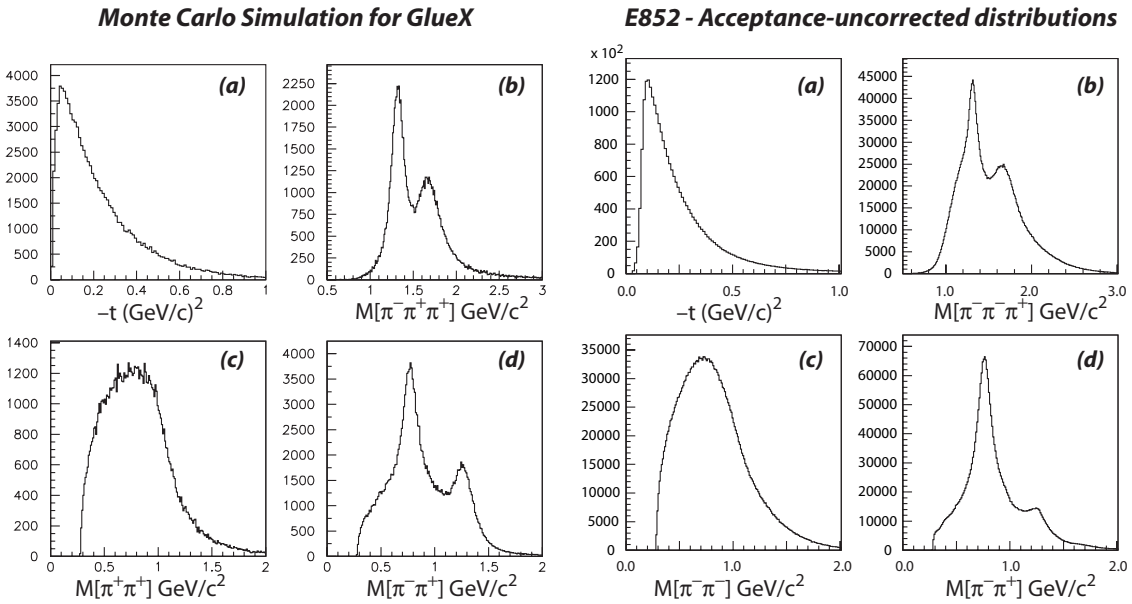

Figure 1.18: Physics distributions for the 3π final state. The left-hand plots are for simulated GlueX $\pi^+\pi^+\pi^-$ data while the right hand plots are for E852 [38] $\pi^-\pi^-\pi^+$ data.

Going beyond this, there have a been a number of studies using the simulated GlueX data to carry out specific amplitude analysis studies. The earliest of these is reported in reference [39] and reports on a

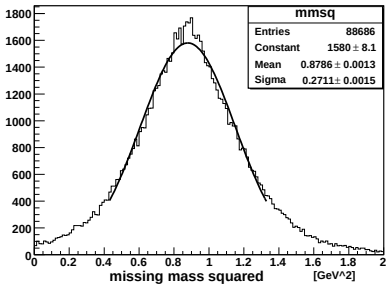

Figure 1.19: Distribution in missing mass squared recoiling against the 3π system for the Monte Carlo sample after resolution smearing. The distribution is centered at m_n^2 and the σ for the Gaussian fit (solid curve) is 0.27 $(\mathrm{GeV}/c^2)^2$. The corresponding E852 missing mass squared distribution had a σ of 0.31 $(\mathrm{GeV}/c^2)^2$.

double-blind study of the 3π reaction. This work used a parameterized Monte Carlo (MCFast[1]). In this first study, a linearly polarized photon beam using an unknown cocktail of t-channel generated mesons which decay to 3π was produced. These events were then given to the analysis team who carried out an analysis similar to that done by E852. In the end, the team found the seven amplitudes included in the generator and excluded about ten other amplitudes based on no observed signal at the sub percent level. The results for such a fit for 100% linearly polarized photons are shown in Figure 1.20. In this fit, a comparison is made between the generated data and the Monte Carlo corrected data. In the 3π channel, the acceptance corrections are fairly small. The data shown are only for the positive reflectivity solutions, but a more or less identical set for the negative reflectivity are also produced. While visible, the acceptance effects are small, and do not hinder the extraction of the partial waves. This original study was later extended by degrading the detector performance at the level of detector resolution, gaps in the detector, and distorted magnetic fields [40]. This latter study indicated that at the level things were simulated, the analysis results were robust against degradations of the detector.

Since those original studies, a realistic (GEANT-based) simulation of the GlueX detector and reconstruction software have been developed. In particular, concerns have been raised that the original studies over-estimated the effects of realistic tracking software. This software has been discussed in section 1.5 and its performance is quite similar to the results obtained from the early fast simulations. We have also developed new fast simulation tools based on the performance of the GlueX software that are now used to carry out studies. One of these studies is to reproduce the original 3π amplitude analysis work. However, given the performance of the actual GlueX software, most of the results of the earlier amplitude analysis studies are still valid. The key point of those studies are that with the detector resolutions and performance and using realistic reconstruction software, it is possible to carry out an amplitude analysis that is sensitive to reactions that are only a few percent of a given final state.

1.9 Diffractive ρ production

There have been a number of studies of s-channel helicity conservation in diffractive vector meson production [19] [37]. This might be a tool for monitoring the degree of linear polarization for GlueX. The helicity angles ($\cos\theta_H$ and ϕ_H) are the pion decay angles defined in the ρ rest frame where the $\hat{z}$ is along the original ρ direction, $\hat{y}$ is normal to the ρ production plane, and $\hat{x} = \hat{y}x\hat{z}$

Events were generate assuming s-channel helicity conservation with a 40% linearly polarized beam at 9 GeV. The acceptance in the helicity angle distributions for a forward angle cut of 1° and 2° is shown in

[1]The MCFast program was written at FermiLab for use by the BTeV experiment. It allowed for both fast simulation and pseudo reconstruction of events with the ability to input reconstruction efficiencies and to get good estimates of reconstruction errors. The GlueX amplitude analysis work was carried out while one of the developers of the code was on the faculty of CMU. After the BTeV experiment was cancelled, the support for the package ended and with rapid changes in compilers and software, it quickly became nearly impossible to maintain and was dropped as a GlueX package in late 2004.

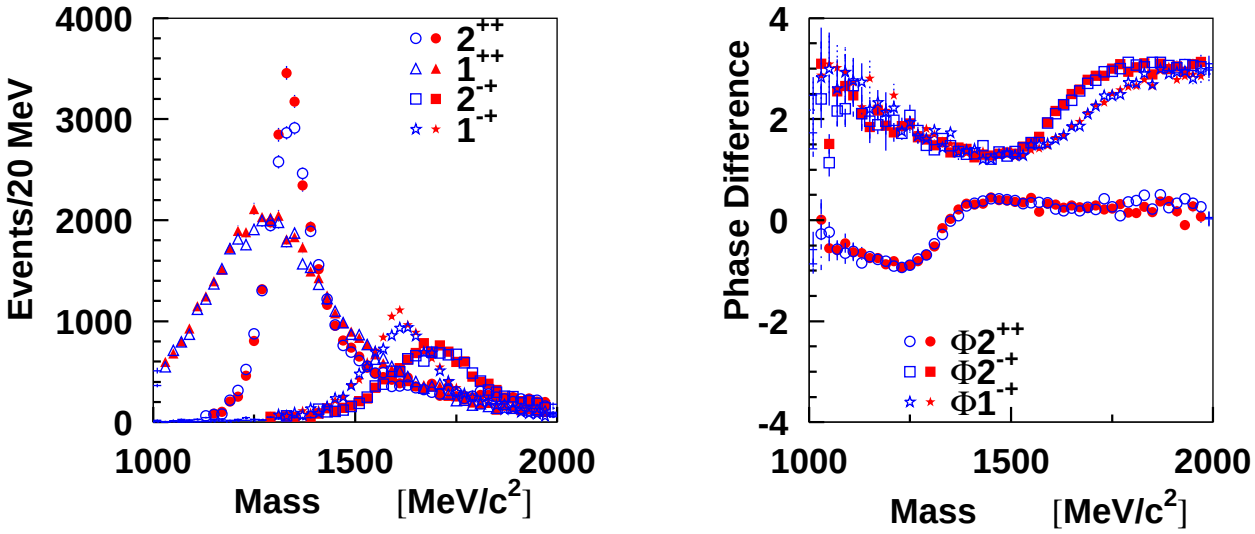

Figure 1.20: These fits compare generated data (solid shapes) to data that has been run through the GlueX McFast Monte Carlo, (open figures). The left figure compares the fits to the intensities of four waves, while the right figure shows the phase differences between the listed waves and the 1^{++} wave.

Figure 1.21. The distortion in the ψ_H distribution is several, especially in going from the 1° cut to the 2°. Acceptance corrections can be made but the knowledge of the efficiency and acceptance as a function of the angular cut have to very well understood. In order to understand the kinematics associated with the ρ decay, we show the mapping from LAB frame quantities to helicity frame quantities in Figure 1.22. Monitoring linear polarization using ρ decays will be a challenge.

1.10 Conclusions

1. Complete detection of final states involiving charged particles and photons are necessary for carrying out the broad program in gluonic excitation planned for GlueX.

2. The detection and measurement of π^0 and η mesons with adequate acceptance and resolution is essential for mapping the spectrum of exotic hybrid mesons.

3. Photoproduction at 9 GeV is expected to provide a rich hunting ground for exotic mesons. What little data on photoproduction exists at these energies provides almost no information on final states with multi-neutrals.

4. Fixed target photoproduction imposes a solenoidal geometry for the detector (see Figure 1.1), including cylindrical tracking (CDC) and calorimetry (BCAL) and circular planar tracking (FDC) and calorimetry (FCAL).

5. Calorimeters with requirements similar to BCAL and FCAL have been built and operated. The KLOE calorimeter provides guidance for BCAL and the lead glass calorimeter used in E852 and RadPhi provides guidance for FCAL.

6. The tracking specifications for the CDC and FDC allow us to reconstruct charged particles and make cuts on event purity that are at least as goos as other successful spectroscopy experiments.

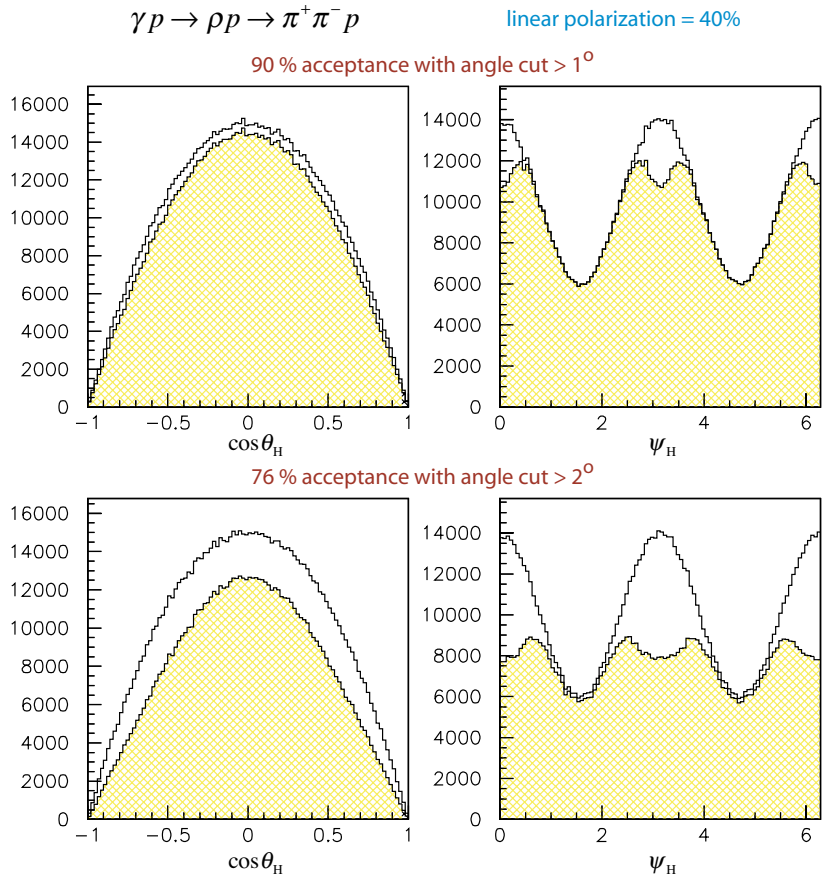

Figure 1.21: GlueX acceptance in the ρ helicity angles assuming 40% linear polarization for the photon beam. The top two plots are for a LAB angle cut of 1° and the bottom two for a LAB angle cut of 2°.

7. A version of PYTHIA, tuned to agree with what is known about photoproduction at GLUEX energies, provides us with guidance on the angular and energy spectra of photons illuminating BCAL and FCAL. These studies indicate that the planned coverage and granularity are adequate.

8. Simulations of GLUEX signature reactions leading to final states such as $\eta\pi^0 p$, $b_1\pi p$, ϕp and $3\pi p$ provide guidance on what is required for energy threshold and energy and position resolution for photons and momentum resolution for charged particles.

9. Achievable mean-time resolution for BCAL is adequate for π/p separation but not for π/K separation.

10. The overall particle identification system in conjunction with global fitting is suffcient to carry out the part of the GLUEX exotic program involving non-strange final states and to start looking at some final states with kaons.

11. The ultimate identification of final states with strange particles will involve an addition Cherenkov detector (probably RICH) downstream of the FDC packages but in front of the time-of-flight wall.

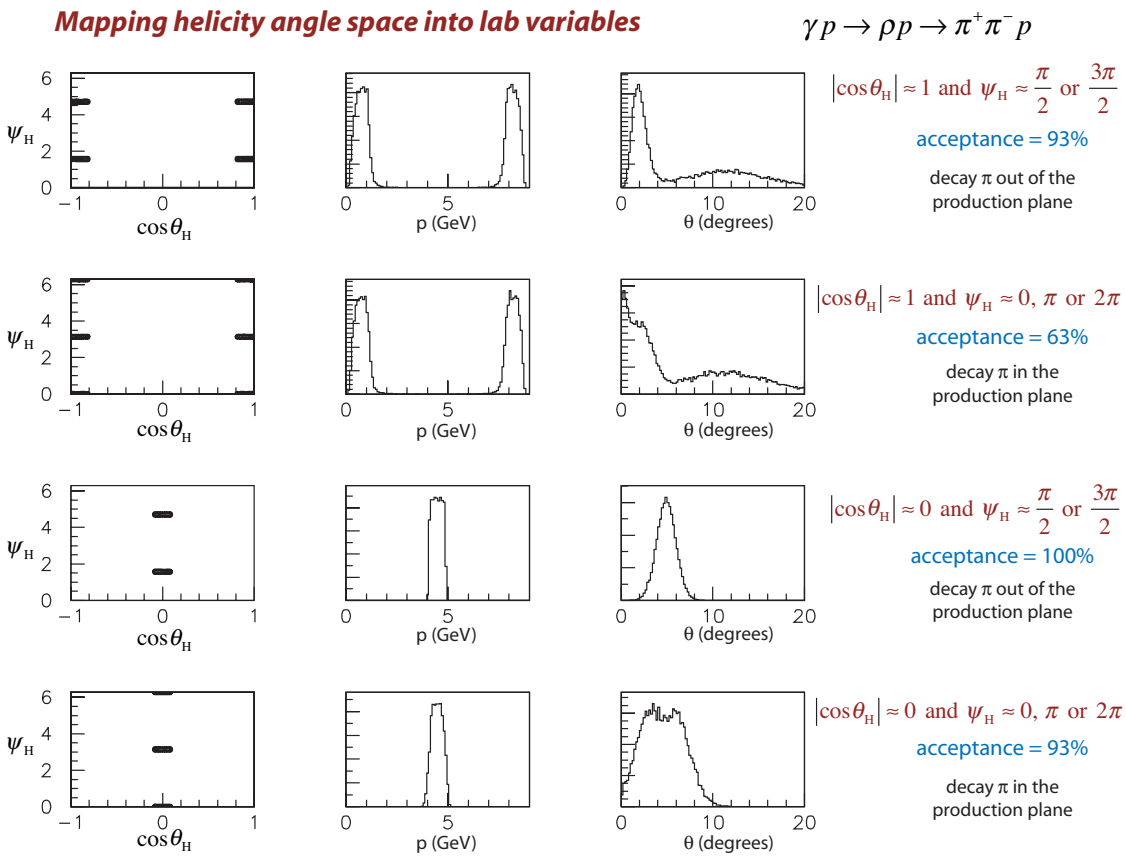

Figure 1.22: The four plots on the left show regions in the ψ_H versus $\cos\theta_H$ plane and the plots in the middle show the corresponding range of LAB momentum and the right column of plots show the corresponding range in LAB angle. The acceptance numbers are what result for these regions when the requirement $\theta_{LAB} > 1^\circ$ is imposed.

References

[1] M. Adinolfi et al. The KLOE electromagnetic calorimeter. *Nucl. Instrum. Meth.*, A482:364–386, 2002.

[2] Hi Wally -

I will most likely be driving to Jefferson lab at that time. Can we do it during the lunch or coffee breaks of the GlueX workshop on either Thursday or Friday?

thanks – Curtis M. Adinolfi et al. The KLOE electromagnetic calorimeter. *Nucl. Instrum. Meth.*, A494:326–331, 2002.

[3] B. B. Brabson et al. A study of two prototype lead glass electromagnetic calorimeters. *Nucl. Instrum. Meth.*, A332:419–443, 1993.

[4] R. R. Crittenden et al. A 3000 element lead-glass electromagnetic calorimeter. *Nucl. Instrum. Meth.*, A387:377–394, 1997.

[5] R. T. Jones et al. A bootstrap method for gain calibration and resolution determination of a lead-glass calorimeter. *Nucl. Instrum. Meth.*, A566:366–374, 2006.

[6] R. T. Jones et al. Performance of the RADPHI detector and trigger in a high rate tagged photon beam. *Nucl. Instrum. Meth.*, A570:384–398, 2007.

[7] C. A. Meyer and Y. van Haarlem. The GlueX Central Drift Chamber. Technical report, GlueX Document, 2008. GlueX-doc-990-v5.

[8] D. S. Carman and S. Taylor. Forward Drift Chamber Technical Design Report. Technical report, GlueX Document, 2007. GlueX-doc-754-v5.

[9] Gunnar S. Bali et al. Static potentials and glueball masses from QCD simulations with Wilson sea quarks. *Phys. Rev.*, D62:054503, 2000.

[10] Y. Nambu. Technical report, U. of Chicago Report No. 70-70, 1970.

[11] Nathan Isgur and Jack E. Paton. A Flux Tube Model for Hadrons in QCD. *Phys. Rev.*, D31:2910, 1985.

[12] Claude W. Bernard et al. Exotic mesons in quenched lattice QCD. *Phys. Rev.*, D56:7039–7051, 1997.

[13] Thomas D. Cohen. Quantum number exotic hybrid mesons and large N(c) QCD. *Phys. Lett.*, B427:348–352, 1998.

[14] Eberhard Klempt and Alexander Zaitsev. Glueballs, Hybrids, Multiquarks. Experimental facts versus QCD inspired concepts. *Phys. Rept.*, 454:1–202, 2007.

[15] Andrei Afanasev and Philip R. Page. Photo- and electroproduction of $J^{PC} = 1^{-+}$ exotics. *Phys. Rev.*, D57:6771–6777, 1998.

[16] C. McNeile and C. Michael. Decay width of light quark hybrid meson from the lattice. *Phys. Rev.*, D73:074506, 2006.

[17] W.-M. Yao et al. Review of particle physics. *J. Phys.*, G33:1, 2006.

[18] H. H. Bingham et al. Total and partial γp cross sections at 9.3 GeV. *Phys. Rev.*, D8:1277–1286, 1973.

[19] J. Ballam et al. Vector meson production by polarized photons at 2.8, 4.7 and 9.3 GeV. *Phys. Rev.*, D7:3150–3177, 1973.

[20] Y. Eisenberg et al. Photoproduction of ω mesons from 1.2 to 8.2 GeV. *Phys. Lett.*, B34:439–442, 1971.

[21] Y. Eisenberg et al. Study of high energy photoproduction with positron-annihilation radiation. I. Three-prong events. *Phys. Rev.*, D5:15–38, 1972.

[22] G. Alexander et al. Study of high energy photoproduction with positron-annihilation radiation. II. The reaction $\gamma p \to p\pi^+\pi^+\pi^-\pi^-$. *Phys. Rev.*, D8:1965–1978, 1973.

[23] G. Alexander et al. Study of high energy photoproduction with positron-annihilation radiation. III. The reactions $\gamma p \to p2\pi^+2\pi^-\pi^0$ and $\gamma p \to n3\pi^+2\pi^-$. *Phys. Rev.*, D9:644–648, 1974.

[24] T. Sjöstrand, S. Mrenna, and P. Skands. Pythia 6.4 Physics and Manual. Technical report, Lund University, 2006. hep-ph/0603175 and http://www.thep.lu.se/~torbjorn/Pythia.html.

[25] A. Dzierba. Comparing Pythia Simulations with Photoproduction Data at 9 GeV. Technical report, GlueX Document, 2007. GlueX-doc-856-v1.

[26] J. Ballam et al. Energy dependence of the reaction $\gamma p \to \rho^-\Delta^{++}$. *Phys. Rev.*, 26:995–997, 1971.

[27] N. Kolev et al. Dependence of the spatial and energy resolution of BCAL on segmentation. Technical report, GlueX Document, 2007. GlueX-doc-659-v2.

[28] B. Leverington. Analysis of the BCAL beam tests. Technical report, GlueX Document, 2007. GlueX-doc-804-v4.

[29] R. Lindenbush. A study of the reaction $\pi^- p \to \eta\pi^0 n$ at 18 GeV/c. Ph. D. Thesis - Indiana University, 1998.

[30] A. R. Dzierba et al. A study of the $\eta\pi^0$ spectrum and search for a $J^{PC} = 1^{-+}$ exotic meson. *Phys. Rev.*, D67:094015, 2003.

[31] R. T. Jones. Detector Models for GlueX Monte Carlo Simulation: the CD2 Baseline. Technical report, GlueX Document, 2006. GlueX-doc-732-v4.

[32] D. Lawrence and S. Taylor. GlueX Simulation Geometry Version 4.0. Technical report, GlueX Document, 2007. GlueX-doc-853-v8.

[33] D. Lawrence. Track fitting in GlueX: Development Report III. Technical report, GlueX Document, 2007. GlueX-doc-761-v2.

[34] H. Wirth, *et al.* (The JETSET Collaboration). Particle Identification with the JETSET Straw Chambers. Nucl. Instrum. Methods A**367**, 248, (1995).

[35] M. Bellis. Technical report, GlueX Document, 2008. GlueX-doc-971-v1.

[36] J. Ballam et al. Vector meson production by polarized photons at 2.8, 4.7 and 9.3 GeV. *Phys. Rev.*, D7:3150, 1973.

[37] K. Schilling, P. Seyboth, and G. Wolf. On the Analysis of Vector Meson Production by Polarized Photons. *Nuc. Phys.*, B15:397 1970.

[38] A. R. Dzierba et al. A partial wave analysis of the $\pi^-\pi^-\pi^+$ and $\pi^-\pi^0\pi^0$ systems and the search for a $J^{PC} = 1^{-+}$ meson. *Phys. Rev.*, D73:072001, 2006.

[39] The Hall D Collaboration, (R. Clark *et al.*). A Search for QCD Exotics Using a Beam of Photons. The GlueX Design Report, version 4, November 2002. GlueX-doc-58.

[40] P. Eugenio, J. Kaditz, C.A. Meyer and B. Zaroukian. A Study of leakage in Partial Wave Analysis for the HallD Detector at Jefferson Lab GlueX-doc-51, December 2001.